applied sciences

MDPI

Article

Tensile Specimen Circular Grid Pattern and AI-Based Strain Calculation Method

Sarang Yi [1], Daeil Hyun [1] and Seokmoo Hong [2,3,*]

[1] Department of Future Convergence Engineering, Kongju National University, Cheonan 31080, Republic of Korea; olluv@smail.kongju.ac.kr (S.Y.); hdi0530@gmail.com (D.H.)
[2] Department of Future Automotive Engineering, Kongju National University, Cheonan 31080, Republic of Korea
[3] Institute of Green Car Technology, Cheonan 31080, Republic of Korea
* Correspondence: smhong@kongju.ac.kr; Tel.: +82-(0)41-521-9268

Abstract: During tensile testing of materials, strain measurement is conducted using either contact or non-contact methods. Contact methods offer high accuracy and precision but are limited by the specimen's thickness and dimensions, whereas non-contact methods minimize damage to thin specimens and allow measurements in various environments, though they require longer preparation and calculation times. This paper proposes a circular grid marking pattern and a strain prediction algorithm using artificial intelligence (AI), which simplifies the preparation process and allows strain prediction without additional equipment. The circular grid pattern can be arranged in various configurations from 1 × 5 to 5 × 7, and a laser marker, which requires minimal time, was used to engrave the pattern on the specimen to shorten the preparation time. The AI model, trained on image-based data, enables strain calculation regardless of the specimen's gauge length and size, and allows measurement of local strain as well as gauge-length strain. The reliability of this concept was verified by applying it to tensile testing.

Keywords: artificial intelligence (AI); grid circle pattern; image processing; measurement strain; tensile test

Citation: Yi, S.; Hyun, D.; Hong, S. Tensile Specimen Circular Grid Pattern and AI-Based Strain Calculation Method. *Appl. Sci.* **2024**, *14*, 7330. https://doi.org/10.3390/app14167330

Received: 8 July 2024
Revised: 8 August 2024
Accepted: 16 August 2024
Published: 20 August 2024

1. Introduction

1.1. Research Background

Historically, the invention or development of new materials has driven the advancement of industrial technologies. Particularly, metal materials have long been used in various fields and continue to be subjects of ongoing research. Recently, in the mobility sector, where efficiency is paramount, composite or metal materials with high strength and stiffness are used [1]. However, defects, such as fractures and wrinkles (cracks) in metal components, can lead not only to personal injuries but also to significant economic losses. Therefore, to establish design safety standards for metal components, it is important to understand the physical properties of the formed shapes, such as thickness, spring-back, and residual stress [2]. Finite element analysis is commonly used to understand the physical properties occurring during the forming of metal materials. When the production conditions of the metal (such as composition and heat treatment) are standardized, the reliability of numerical results regarding the metal's physical properties can be ensured through information obtained from extensive testing. However, for newly developed metals, material tests, such as tensile tests, are required to verify the reliability of numerical results by obtaining the material's physical properties [3].

The tensile testing procedure involves mounting a specimen processed to standard specifications in a tester and measuring the stress and strain generated when it is subjected to tensile stress at a constant speed. Strain measurement methods can be divided into contact methods using gauges and non-contact methods using cameras or sensors.

Contact measurement methods include mechanical extensometers, electrical resistance extensometers (strain gauges), and inductive extensometers, all of which measure displacement by being directly attached to the specimen [4]. Non-contact measurement methods encompass video measurement, laser measurement, digital image correlation (DIC), and ultrasonic measurement. DIC, in particular, is noteworthy for its ability to measure 3D deformations and acquire data from multiple points, making it suitable for use in extreme temperatures and large deformation environments. Additionally, DIC can measure strain in the specimen's width and thickness directions, not just in the length direction. This method calculates strain by analyzing changes in the pattern applied to the specimen's surface and can track local strain at specific points, such as just before necking or fracture occurs [5–7].

Mechanical extensometers are attached to the specimen to provide highly reliable measurements and are less affected by environmental changes, such as ambient light or temperature. However, their measurement range can be exceeded by material elongation, and they may be difficult to attach to thin sheets [8]. Strain gauges can measure fine deformations through electrical resistance but are significantly affected by temperature changes [9]. Inductive extensometers can accurately measure fine deformations and are usable in high-temperature and extreme environments, although they are influenced by external electric fields. Contact measurement methods measure deformation based on the gauge length specified in tensile specimen standards, making it challenging to accurately analyze strain at actual fracture locations [10].

Non-contact measurement methods do not require physical contact with the specimen, preventing deformation caused by the measuring instrument in thin-sheet specimens and allowing usage under various environmental conditions, including different temperatures, pressures, and vacuum [11]. However, non-contact methods require expensive equipment, such as high-speed high-resolution cameras, lasers, ultrasonic devices, and image analysis software. They are also sensitive to optical conditions, such as lighting, reflection, and dust. Specifically, DIC requires high computing performance to measure strain by analyzing correlations over the entire image area captured by the camera and necessitates the application of a speckle pattern on the specimen surface [5]. Additionally, to measure the strain on the tensile specimen surface using DIC, a speckle pattern must be applied to the specimen using spray, allowing the tracking of image changes. However, this application process is time consuming and, during the drying process, the paint may peel off depending on the specimen's surface roughness and material properties, making measurement impossible.

The technical issues of the various measurement methods discussed can be summarized as follows. Contact methods offer high accuracy and precision but are limited by the specimen's thickness and dimensions. Non-contact methods minimize damage to thin specimens and allow measurements in various environments, but they require expensive equipment, are sensitive to environmental conditions, and involve lengthy preparation and calculation times. Therefore, a need exists for a strain measurement method that reduces calculation and preparation time and does not require additional equipment.

1.2. Literature Review

Because these contact and non-contact material property measurement methods have individual advantages and disadvantages concerning specimen shape, environment, time, and cost, many researchers have proposed ideas to overcome these drawbacks. Ko et al. [12] proposed a theoretical formula to predict the measurement performance of strain gauge sensors based on specimen deformation through experiments and finite element analysis, showing that measurement values can be predicted by finite element analysis. Some studies have been conducted to improve strain measurement accuracy at cryogenic temperatures [13,14]. The results demonstrated that contact measurement methods could be used even in extreme environments, such as cryogenic conditions. Xu et al. [15] proposed a method to split the laser beam into two independent sections to improve accuracy and resolution, demonstrating that this method minimizes uncertainties and avoids data loss

even in large deformations. Kersemans et al. [16] proposed a method using harmonic ultrasonic backscatter polar scan (H-UBPS) to measure the cross section of specimens without sample preparation, achieving accuracy similar to commercial methods. Li et al. [17] proposed chain subset-based DIC technology and a modified second-order shape function (MSSF) to automate tensile tests, increasing measurement accuracy and reducing calculation time. Bulava et al. [18] proposed automating strain measurement using a high-resolution camera, confirming that pattern matching and specifying particular ROIs can reduce calculation time.

Kim et al. [19] proposed using in situ SEM and artificial intelligence algorithms to restore low-resolution images to high-resolution, improving strain measurement accuracy. Liu et al. [20] applied machine learning techniques, including long short-term memory (LSTM) and convolutional neural networks (CNN), to predict the properties of additively manufactured metamaterials. Shim et al. [21] used deep learning to predict the mechanical properties of recycled composites, though the study was limited to recycled CFRTP (Carbon Fiber Reinforced Plastic) materials. Karathanasopoulos et al. [22] proposed an algorithm to identify fractures during tensile testing using a CNN. This method confirmed that using machine learning methods and image subset generation techniques can automatically locate fracture positions. Castro et al. [23] measured strain using mechano-chromic sensors and machine learning, proposing a load prediction algorithm based on color changes due to applied loads. However, they noted limitations in resolution. Yang et al. [24] used deep learning to compensate for lost strain data in DIC measurements but found that the method could not be applied when the specimen's deformation was non-uniform. Lee [25] proposed a method to measure the strain between two marked points on the gauge length using the DIC technique but confirmed that it could not measure local strain.

As is evident from these previous studies, contact measurement methods have been researched to ensure accuracy in extreme environments but remain challenging to apply to thin sheets [12–14]. Additionally, non-contact measurement methods have been studied to improve accuracy and reduce calculation times, but they still require preparatory work [15–25]. Many researchers have proposed methods to improve the accuracy and efficiency of DIC in strain calculation. Although the DIC method is currently considered the best for material property measurement, the significant time required for spray pattern preparation and the calculation time still need improvement. Moreover, accurately measuring the strain at the fracture site is crucial for predicting fracture behavior in metal materials [26], yet research in this area remains insufficient.

1.3. Motivation and Novelty

Traditional tensile testing methods involve significant time and cost due to preparatory work and equipment setup, limiting their usability in various environments. Therefore, a simplified and efficient method is required to enable usage without environmental limitations. Additionally, to improve strain prediction accuracy and minimize differences due to user proficiency, an automated process that minimizes user intervention is needed. Accurately predicting material behavior and fracture also requires identifying strain at the fracture point, not just at the gauge length.

Thus, this paper proposes a circular grid marking pattern and a strain prediction algorithm using AI, which simplifies the preparation process and allows strain prediction with a single camera without the need for additional equipment. To shorten the preparation time, the circular grid pattern is engraved on the specimen using a laser marker, which requires minimal time. Applying this method to tensile testing demonstrated the advantages of this study's concept. The proposed circular grid marking pattern can be applied regardless of the specimen's shape. Strain is measured using an image-based AI model, allowing calculation regardless of the specimen's gauge length and size, and enabling the measurement of local strain as well as gauge-length strain. The strain predicted by the AI model is automatically used to calculate the stress–strain curve, elastic modulus, and elongation.

The structure of this paper is as follows. Section 2 introduces the theoretical background of the strain measurement calculation and method that utilizes the circular grid, as well as the image preprocessing and AI model used to detect only marking images and determine strain. Section 3 describes the tensile test procedure, including the shape and formation method of the circular grid pattern proposed in this study. The circular grid pattern's strain prediction accuracy differences were analyzed according to specimen size and camera specifications. Section 4 explains the data generation method for training the proposed strain prediction algorithm and the AI training conditions. Section 5 covers the results and analysis of strain prediction accuracy with variations in the circular grid pattern, formation method, and AI training. Finally, Section 6 summarizes conclusions regarding the proposed circular pattern method and AI strain prediction.

2. Theoretical Background

2.1. Material Test

Formability refers to the ability or degree to which a material can undergo plastic deformation and is used to assess the material's suitability for forming. To evaluate formability, tests are conducted to replicate the deformation modes that the material undergoes in actual processes, among which the tensile test is the most widely used method. The circular grid pattern proposed in this paper is applied for forming-limit tests [27–29]. As shown in Figure 1, the nominal and true strains of the deformed circles in the major (*1*) and minor (*2*) directions can be calculated using Equation (1). This paper proposes applying the circular grid pattern to tensile test specimens, considering only the major direction strain to calculate the stress–strain curve in tensile tests.

$$\text{Engineering strain}: \; e_1 = \frac{a - d_0}{d_0}, \; e_2 = \frac{b - d_0}{d_0}$$

$$\text{True strain}: \; \varepsilon_1 = ln\frac{a}{d_0} = \ln(1 + e_1), \; \varepsilon_2 = ln\frac{b}{d_0} = \ln(1 + e_2) \tag{1}$$

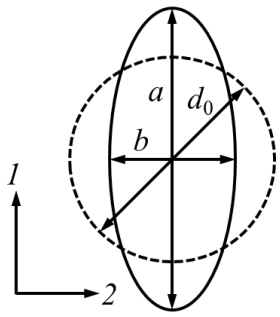

Figure 1. Major and minor direction strains of the circular grid pattern.

2.2. DIC Measurement Method

The DIC method used to verify the proposed shape and prediction algorithm creates an irregular speckle pattern on the specimen, as shown in Figure 2, comparing pre-deformation and post-deformation images to calculate the entire specimen area. Compared to the traditional method of marking two points on the specimen and using an extensometer to measure strain, it provides detailed information, such as directional strain and local strain. Additionally, because it captures images in real time during the test, it allows for tracking the deformation path and predicting the strain just before necking or fracture occurs.

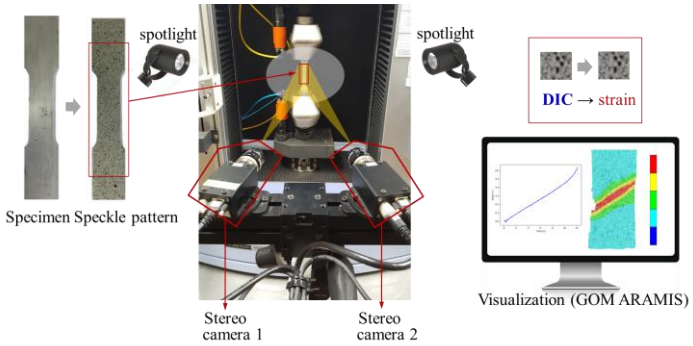

Figure 2. DIC measurement method.

3D measurement equipment uses two stereo cameras to measure the three-dimensional distance of an object, requiring sufficient space to ensure an appropriate field of view. 3D measurements are accurately performed at the point where the cameras and the object form a triangle, resulting in a limited measurement area. The setup requires at least 30 min due to the need to calibrate dozens of images, and the equipment is expensive, depending on the camera resolution and measurement area. In contrast, 2D measurements can be performed with a smartphone camera, but there can be distortion at the edges, and accurate measurements require the object and camera to be perpendicular. This paper assumes that the 2D camera and the target object are perpendicular to each other.

2.3. Image Preprocessing

Image-based strain measurement methods are divided into 2D and 3D methods, with 3D DIC methods generally being applied for experiments. In this study, 2D was used to simplify the tensile test; because the material was a thin sheet, the difference between 2D and 3D was negligible, so thickness direction strain was ignored. The tensile test was recorded on video and images for the training data were generated from the test video, with necessary data extracted by image preprocessing.

To extract only single circles from the circular grid pattern in the video recorded during the tensile test, image binarization was applied. Image binarization [30], as shown in Figure 3, converts the image into two colors, 0 and 255, and was applied in this study to reduce noise. Image binarization generally sets pixels above a certain threshold to 0 and the others to 255. In this case, the generated images had white objects on a black background. Given image A and structural element B, dilation and erosion are defined as in Equation (2). In Equation (2), B_z is the transformation of B by vector z, representing the symmetry of $\hat{B}$.

$$\begin{aligned} A \bigoplus B &= \{x | [(\hat{B})_z \cap A] \neq 0\} \\ A \odot B &= \{x | (B)_z \subseteq A\} \\ A \circ B &= (A \odot B) \bigoplus B \\ A \cdot B &= (A \bigoplus B) \odot B \end{aligned} \tag{2}$$

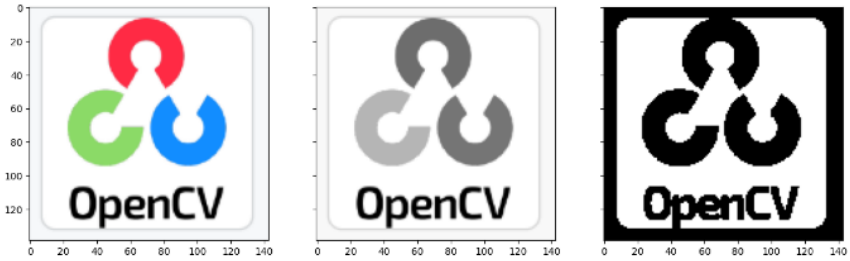

Figure 3. Image binarization.

After reducing noise and extracting only circles through image binarization, the image size typically consists of approximately 20 × 20 pixels. This size represents the pixel space where the circular pattern exists within a 1920 × 1080 size when adjusting the camera position considering the elongation of the material during the tensile test. The circular pattern exists in a relatively localized area compared to the overall image size so, even when captured at high resolution during the tensile test, only low-resolution images can be obtained. The lower the image resolution, the fewer pixels are available to represent the deformation of the circle. For example, if a circle with a diameter of 10 mm is composed of pixels with sizes of 1 × 1 mm and 2 × 2 mm, when the circle deforms to 12 mm, the 1 × 1 mm pixels would show 2 pixels, while the 2 × 2 mm pixels would show 1 pixel, resulting in loss of deformation information. To overcome this issue with low-resolution images, super resolution was applied to obtain high-resolution images. Super resolution converts low-resolution images to high-resolution images through AI training, as shown in Figure 4 [31].

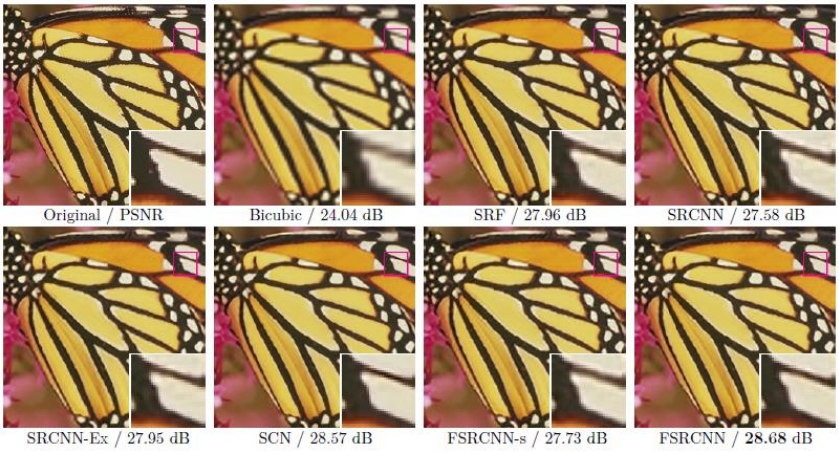

Figure 4. Example of super resolution application [31].

2.4. AI Training Model

AI algorithms that classify and predict specific values based on images generally use a CNN structure. A CNN is an artificial neural network comprising one or several convolutional layers and traditional artificial neural network layers, capable of extracting high-dimensional image information compared to conventional image processing methods. Unlike a fully connected neural network, a CNN maintains the shape of the input and output data for each layer, effectively recognizing features from adjacent images while preserving image spatial information. Using shared parameters for filters, it requires significantly fewer learning parameters compared to a general artificial neural network. Image classification and prediction algorithms based on CNN structures include Visual Geometry Group (VGG), ResNet, and MobileNet.

VGG [32] is distinguished as VGG16 or VGG19 according to the number of convolutional layers, with the model structure comprising C and E, as shown in Figure 5. It repeatedly applies convolutional layers with filtering techniques to the input image, the ReLU nonlinear activation function, and pooling layers that reduce the size of the image data. Then, the data are vectorized through the fully connected (FC) layer and normalized through the softmax activation function.

ResNet (Residual Network) [33], unlike VGG, is composed of blocks, as shown in Figure 5. By residual mapping, which adds values that have passed through convolutional layers to those that have not, it mitigates overfitting and parameter vanishing problems as the layer depth increases [20]. ResNet's layer structure uses convolutional layers with 7 × 7 filters and 3 × 3 max pooling.

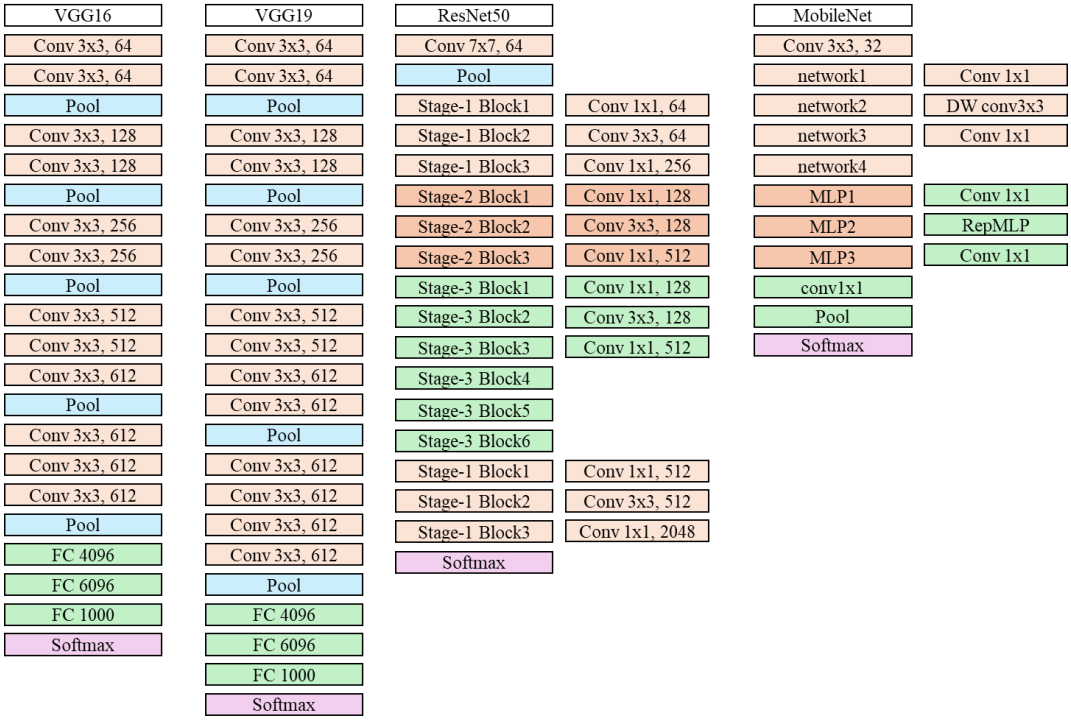

Figure 5. AI model structures VGG [32], ResNet50 [33], and MobileNetV2 [34].

MobileNetV2 [34] is a neural network designed for efficient computation in resource-constrained environments such as smartphones and other mobile devices, reducing the number of parameters and computation requirements compared to traditional CNNs. MobileNet applies depth-wise separable convolutions, as shown in Figure 5, and calculates spatial direction depth-wise convolutions and channel direction point-wise convolutions separately before combining them. Because different filters are applied to each channel, the number of output channels remains the same as the number of input channels.

3. Circular Grid Pattern

3.1. Circular Grid Pattern Shape

The tensile specimen used in this study applied the KS B 0801 standard [35], as shown in Figure 6. The material used was STS (stainless steel) 304 with a thickness of 3 mm. In this context, T represents thickness, L is the gauge length, r is the parallel length, R is the radius, and B is the grip width, which are 3 mm, 50 mm, 60 mm, 20 mm, and 20 mm, respectively. The specimen was processed using laser cutting.

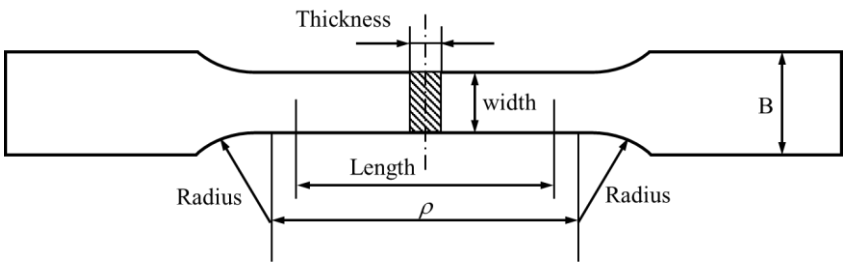

Figure 6. Tensile specimen diagram.

This paper proposes a circular grid pattern to replace the speckle pattern used in traditional DIC. The proposed circular grid pattern can measure strain from the gauge length to the local strain at the fracture site. As shown in Figure 7, the pattern consists of grids with circles arranged in configurations, such as 1×5, 3×5, 1×7, and 5×7. The

pattern position is based on the center of the parallel section of the tensile specimen. There must be at least one row, and at least three circular markings must be formed in the tensile direction. It should consist of at least two circles indicating the gauge length and one or more positioned at the specimen center. However, because fractures do not consistently occur at the center, at least five circular markings should be formed in the tensile direction to account for the fracture location. Accordingly, the 1×5 circular grid is the minimum pattern proposed in this study, and the minimum circle size can be selected on the basis of the material strain and camera specifications. This is a crucial factor because of the area within the camera frame where the tensile specimen deforms must be specified, considering both the initial state and the deformation. The tensile specimen moves further from the camera as it strains, and the extracted tensile specimen area becomes a low-resolution image as the camera moves away. Hence, it is necessary to examine the minimum pixel size of the circle that can be calculated for strain.

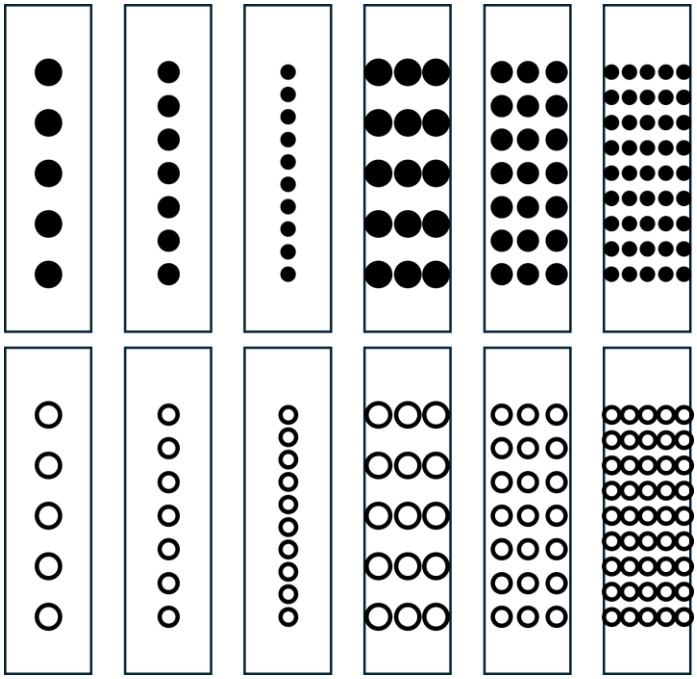

Figure 7. Circular grid pattern examples.

3.2. Pattern Formation Method

The circular grid pattern can be represented using laser marking. Here, the laser marking was embossed, not affecting material behavior, and was engraved in black for clear distinction from the specimen in image processing. This method is called black marking, and it involves etching a dark shadow on the surface without removing material. Unlike regular laser marking, the heat or chemical reaction generated during black marking has minimal impact on the material. Therefore, the material deformation caused by laser marking was considered negligible in this study. An ideal small fiber laser marker LG-20P was used for laser marking, with conditions of 300 mm/s and 50 Hz on the STS 304 surface. This marking machine can be applied to metal materials, such as stainless steel, copper, aluminum, iron, gold, and silver, as well as certain plastics, like PET, PP, PVC, and ABS, making it applicable to materials beyond those used in this study. Additionally, the time required to mark the circular grid shown in Figure 7 on the specimen depicted in Figure 6 is approximately 20 s on average.

4. Image Data and Training Procedure

4.1. Image Data Generation Method

Circular grid pattern images were extracted by recording the tensile test on video using a digital single-lens reflex (DSLR) camera. Additionally, to validate the proposed algorithm, data measured with the traditional DIC method were compared, and lighting was set up to capture images without reflections by reducing specimen reflection.

From the video of the tensile test process, circular image data were extracted from each frame. The procedure for extracting circular image data is shown in Figure 8, where the tensile specimen was identified using Yolo v4 training on the recorded original image, and the ROI of the detected tensile specimen was designated. Image binarization was applied for contour detection, and image inversion and morphological operations, specifically open operations, were performed to reduce unnecessary noise. To detect only the contours of the circular grid pattern, the pixel size detected was limited by the ratio of the gauge length to the circle diameter. As a result, the circular grid pattern was detected as shown in the pattern ROI of Figure 7, and the circular image ROI was obtained using the coordinates acquired at that time. The acquired circular ROI image was extracted from the original image to prevent information loss during the image preprocessing step that detects the circular pattern and was binarized for training application. The extracted circular images had different sizes depending on the size of each circle. For AI training, all images must be the same size, so the extracted circular images must be resized uniformly. Simply enlarging the extracted images to match the size can deform the circular image itself, leading to different results in strain calculations. To prevent this problem, the circle detected in the first frame of the video was designated as the initial circular image, and a white image twice the diameter of the circle was created. The binarized circular image was combined with the generated white image centered to create an image of the same size without losing the information about the circle size. Additionally, the images used for training were enlarged to a size of 112 × 112; because the resolution of the extracted circular image was low at about 20 × 20 pixels, super resolution was applied to obtain additional high-resolution images. From the images obtained through the preprocessing step, the initial circular image detected in the first frame and the circular images detected in frames 2 to N were used as input data for the AI application.

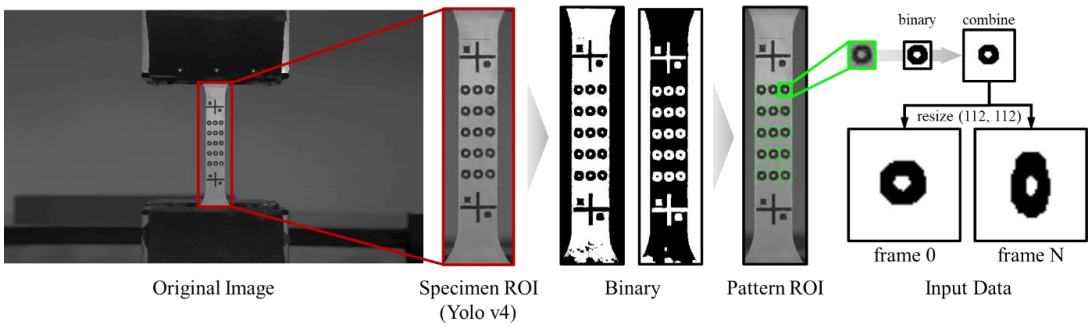

Figure 8. Image preprocessing.

4.2. AI Training Procedure

In the strain prediction algorithm, the input data are the images of the undistorted circle from the initial frame and the distorted circles from subsequent frames, with the output being the corresponding strain values. Therefore, the length in the y-axis direction was measured for the image data obtained from image processing as described in Section 4.1, and each image was labeled with its strain. From the 6450 data points obtained from tensile tests, 70% were used for training, 10% were classified as validation data, and the remaining were used as test data. AI training was obtained with a NVIDIA DGX STATION (Future Automotive Intelligent Electronics Core Technology Center, Cheonan, Republic of Korea).

In AI, the accuracy of prediction results is determined by the coefficient of determination. The coefficient of determination is an indicator of how well the independent variables

explain the dependent variable in a regression model; a higher coefficient indicates that the independent variables explain the dependent variable more effectively. The coefficient of determination is calculated as shown in Equation (3), where y is the observed value, $\overline{y}$ is the mean of the observed values, and $\hat{y}$ is the predicted value.

$$r^2 = \frac{\sum(\hat{y} - \overline{y})^2}{\sum(y - \overline{y})^2} \quad (3)$$

5. Results and Discussion

5.1. AI Training Results

For strain prediction, algorithms with CNN structures were used, including VGG16, VGG19, ResNet50, and MobileNet, and the prediction accuracy of the four structures was compared. Among the AI algorithms compared, VGG16 had the highest coefficient of determination at 0.978. This result confirmed that the VGG structure is more suitable for strain prediction than other networks, as detailed in Table 1. AI training demonstrated that strain prediction based on images is sufficiently possible. This result confirmed that strain can be automatically calculated in tensile tests and that local strain can also be calculated.

Table 1. AI training coefficient of determination.

Model Name	VGG16	VGG19	ResNet50	MobileNet
R^2	0.978	0.974	0.9614	0.904

5.2. Strain According to Resolution

Tensile tests were conducted on the 3 × 5 circular grid array using STS 304 material. The video resolution during the tensile test was 1920 × 1080 (1080p), which was then changed to 1280 × 720 (720p) and 854 × 480 (480p) to analyze the impact of resolution on strain calculation. Strain was calculated for images at each resolution, and the stress–strain curves were compared, as shown in Figure 9. The graph shows that, while calculating strain over the gauge length is not significantly affected by resolution, the accuracy of local strain calculations decreases as resolution decreases. Experiments confirmed that, when the material elongation is 0.7, the image pixel size for the circle must be at least 10 × 10 pixels. To verify the proposed strain prediction algorithm, tensile test data for the predicted material was measured using a 3D DIC device; the calculated stress–strain curve is shown in Figure 9. At this time, (a) represents the strain calculation result for the gauge length, and (b) represents the result for the local strain. The strain for the gauge length is similar to the DIC results regardless of the resolution. However, for local strain, it was confirmed that, the higher the resolution, the more accurate the calculation. Therefore, it was confirmed that resolution has a significant impact on calculating local strain, and a minimum resolution of 1080p is required.

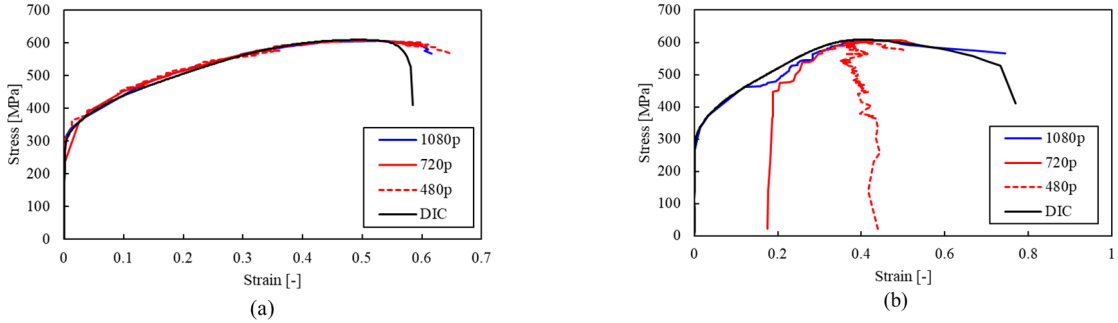

Figure 9. Comparison of DIC and Engineering strain prediction algorithm: (**a**) gauge length, (**b**) local strain.

5.3. Discussion and Contributions

The measurement error between the existing method and the newly proposed method was sufficiently effective at less than 5%, verifying the validity of the proposed method and confirming that it could yield meaningful values. The minimum size criteria for the proposed circular pattern were established. This paper proposes a laser marking method, but other methods can be applied according to the operator's needs. When predicting strain using laser marking and artificial intelligence, it takes approximately 1 min and 30 s. This is a significant reduction compared to the traditional DIC method, which takes around 1 h and 30 min for spray application/drying and calculation time. This demonstrates that the proposed method is more efficient in terms of time.

The results show that, compared to traditional tensile test methods, the equipment setup for the proposed method is easier, the preparation time is reduced, and the accuracy is similar to that of existing methods. As a result, tensile test automation is feasible, and it is expected that a process for real-time application and versatility across various materials can be developed.

However, because this study was limited to steel materials and tensile tests, there are restrictions on applying it to various other materials and test methods. Additionally, noise was entirely removed from the dataset images for training, leading to reduced accuracy in noisy environments.

6. Conclusions

In this study, a 2D tensile test strain prediction algorithm without time and cost constraints was developed by applying image preprocessing and AI; the prediction accuracy of various algorithms was compared. The research process and results can be summarized as follows.

To reduce the preparation time for speckle pattern application in traditional DIC measurements, a new marking method is proposed, and an algorithm to predict strain based on this marking shape was suggested.

The strain prediction algorithm coefficients of determination were compared for the VGG16, VGG19, ResNet, and MobileNet AI structures; VGG16 exhibited the highest prediction accuracy.

The strain prediction process using AI takes approximately 1 min and 30 s for specimen marking and calculation, confirming its efficiency in terms of time. As a result, tensile test automation was judged to be feasible, and it is expected that a process for real-time application and versatility across various materials can be developed.

Author Contributions: S.Y.: Model design, Methodology, Software, Writing—original draft. D.H.: Writing—modification of draft, Writing—review and editing. S.H.: Supervision, Writing—modification of draft, Writing—review and editing. All authors have read and agreed to the published version of the manuscript.

Funding: This research was funded by Future Automotive Intelligent Electronics Core Technology Center, Cheonan, Republic of Korea.

Institutional Review Board Statement: Not applicable.

Informed Consent Statement: Not applicable.

Data Availability Statement: The original contributions presented in the study are included in the article, further inquiries can be directed to the corresponding author.

Acknowledgments: This work was supported by a research grant of the Kongju National University in 2023. FE results were obtained with a NVIDIA DGX STATION (Future Automotive Intelligent Electronics Core Technology Center, Cheonan, Republic of Korea).

Conflicts of Interest: The authors declared that there are no conflicts of interest.

References

1. Trzepiecinski, T.; Najm, S.M. Current trends in metallic materials for body panels and structural members used in the automotive industry. *Materials* **2024**, *17*, 590. [CrossRef] [PubMed]
2. Wiebenga, J.H.; Atzema, E.H.; An, Y.G.; Vegter, H.; van den Boogaard, A.H. Effect of material scatter on the plastic behavior and stretchability in sheet metal forming. *J. Mater. Process. Technol.* **2014**, *214*, 238–252. [CrossRef]
3. Banergee, D.K.; Iadicola, M.A.; Creuziger, A. Understanding deformation behavior in uniaxial tensile tests of steel specimens at varying strain rates. *J. Res. Natl. Institute of Stand. Technol.* **2021**, *126*, 126050. [CrossRef]
4. Schwarzkopf, E.A. Overview and comparison of noncontacting and traditional contacting extensometers. In *Evaluation of Existing and New Sensor Technologies for Fatigue, Fracture, and Mechanical Testing*; Kang, J., McKeighan, P.C., Dahlberg, G., Kemmerer, R., Eds.; 100 Barr Harbor Drive, PO Box C700; ASTM International: West Conshohocken, PA, USA, 2022. [CrossRef]
5. He, X.; Zhou, R.; Liu, Z.; Chen, S.Y.K.; Li, L. Review of research progress and development trend of digital image correlation. *Multidiscip. Model Mater. Struct.* **2024**, *20*, 81–114. [CrossRef]
6. Peters, W.H.; Ranson, W.F. Digital imaging techniques in experimental stress analysis. *Opt. Eng.* **1982**, *21*, 427–431. [CrossRef]
7. Peters, W.H.; Ranson, W.F.; Sutton, M.A.; Chu, T.C.; Anderson, J. Application of digital correlation methods to rigid body mechanics. *Opt. Eng.* **1983**, *22*, 738–742. [CrossRef]
8. Zhang, S.; Mao, S.; Arola, D.; Zhang, D. Characterization of the strain-life fatigue properties of thin sheet metal using an optical extensometer. *Opt. Lasers. Eng.* **2014**, *60*, 44–48. [CrossRef]
9. Gavrilenkov, S.I. Method of simulating temperature effect on sensitivity of strain gauge force sensor in non-uniform temperature field. In *AIP Conference Proceedings*; AIP Publishing: College Park, MD, USA, 2019. [CrossRef]
10. Yoshihara, H.; Yoshinobu, M. Effects of specimen configuration and measurement method of strain on the sharacterization of tensile properties of paper. *J. Wood. Sci.* **2014**, *60*, 287–293. [CrossRef]
11. Xu, Q.; Wang, X.; Yan, F.; Zeng, Z. Non-Contact extensometer deformation detection via deep learning and edge feature analysis. In *Design Studies and Intelligence Engineering*; IOS Press: Amsterdam, The Netherlands, 2023. [CrossRef]
12. Ko, M.; Lee, T. Performance Characteristics of Sensor Part in Extensometer Using Strain Gauge. *Trans. Korean Soc. Mech. Eng. A* **2019**, *43*, 201–208. [CrossRef]
13. Tabin, J.; Prącik, M. Methods for identifying dynamic parameters of clip-on extensometer–specimen structure in tensile tests. *Measurement* **2015**, *63*, 176–186. [CrossRef]
14. Tabin, J. Strain measurement by means of clip-on extensometers during discontinuous plastic flow at 4 K. *Cryogenics* **2022**, *123*, 103451. [CrossRef]
15. Nie, X.; Song, B.; Loeffler, C.M. A novel splitting-beam laser extensometer technique for kolsky tension bar experiment. *J. Dyn. Behav. Mater.* **2015**, *1*, 70–74. [CrossRef]
16. Kersemans, M.; Allaer, K.; Paepegem, W.V.; Abeele, K.V.D.; Pyl, L.; Zastavnik, F.; Sol, H.; Degrieck, J. A novel ultrasonic strain gauge for single-sided measurement of a local 3D strain field. *Exp. Mech.* **2014**, *54*, 1673–1685. [CrossRef]
17. Li, D.; Cheng, B.; Xiang, S.; Zhou, H. Integrative measurement method for tensile test based on DIC using modified second-order shape function. *Measurement* **2024**, *226*, 114098. [CrossRef]
18. Bulava, J.; Hargas, L.; Koniar, D. Contactless Material Tensil Testing Using a High-Resolution camera. *Computation* **2022**, *10*, 121. [CrossRef]
19. Kim, S.J.; Min, H.G.; Park, J.H.; Kang, D.J. Application of deep learning method for time reduction and precision improvement in displacement measurement during in-situ SEM tensile test. *Measurement* **2024**, *in press*. [CrossRef]
20. Liu, Q.; Wu, D. Machine learning and feature representation approaches to predict stress-strain curves of additively manufactured metamaterials with varying structure and process parameters. *Mater. Des.* **2024**, *241*, 112932. [CrossRef]
21. Shim, Y.B.; Lee, I.Y.; Park, Y.B. Predicting the material behavior of recycled composites: Experimental analysis and deep learning hybrid approach. *Compos. Sci. Technol.* **2024**, *249*, 110464. [CrossRef]
22. Karathanasopoulos, N.; Hadjidoukas, P. Deep learning based automated fracture identification in material characterization experiments. *Adv. Eng. Inform.* **2024**, *60*, 102402. [CrossRef]
23. Castro, L.D.C.; Scabini, L.; Ribas, L.C.; Bruno, O.M.; Oliveira, O.N., Jr. Machine learning and image processing to monitor strain and tensile forces with mechanochromic sensors. *Expert Syst. Appl.* **2023**, *212*, 118792. [CrossRef]
24. Yang, R.; Li, Y.; Zeng, D.; Guo, P. Deep DIC: Deep learning-based digital image correlation for end-to-end displacement and strain measurement. *J. Mater. Process Technol.* **2022**, *302*, 117474. [CrossRef]
25. Lee, S. Analysis of tensile testing errors in metal thin film using the DIC method. *Trans. Korean Soc. Mech. Eng. A* **2020**, *44*, 513–518. [CrossRef]
26. Kim, M.; Gu, B.; Hong, S. Determination of post-necking stress-strain relationship for zirconium low-oxidation based on actual cross-section measurements by DIC. *J. Mech. Sci. Technol.* **2020**, *34*, 4211–4217. [CrossRef]
27. Hsu, Q.C. Comparison of different analysis models to measure plastic strains on sheet metal forming parts by digital image processing. *Int. J. Mach. Tools Manuf.* **2003**, *43*, 515–521. [CrossRef]
28. Ibrahim, J.S.; Prasad, M.J.N.V.; Narasimhan, P.S.K. Effects of foil thickness to grain size (t/d) ratio and prestraining on tensile response, Microformability and Crystallographic texture of ultra-low carbon steel thin foils. *Met. Mater. Int.* **2024**, *30*, 348–359. [CrossRef]

29. Wankhede, P.; Narayanaswamy, N.G.; Kurra, S.; Priyadarshini, A. A portable device for single point strain analysis in sheet metal forming processes. *HardwareX* **2022**, *12*, e00371. [CrossRef] [PubMed]
30. Joshi, O.S. Binary image processing for computation of connected components, image holes and Euler number using graph theory. In Proceedings of the 2018 International Conference on Advances in Communication and Computing Technology (ICACCT), Sangamner, India, 8–9 February 2018; pp. 230–234. [CrossRef]
31. Dong, C.; Loy, C.C.; Tang, X. Accelerating the super-resolution convolutional neural network. In Proceedings of the Computer Vision–ECCV 2016: 14th European Conference, Amsterdam, The Netherlands, 11–14 October 2016; Proceedings, Part II 14. Springer International Publishing: Bael, Switzerland, 2016; pp. 391–407. [CrossRef]
32. Simonyan, K.; Zisserman, A. Very deep convolutional networks for large-scale image recognition. In Proceedings of the International Conference on Learning Representations, Banff, AB, Canada, 14–16 April 2014. [CrossRef]P
33. He, K.; Zhang, X.; Ren, S.; Sun, J. Deep residual learning for image recognition. In Proceedings of the 2016 IEEE Conference on Computer Vision and Pattern Recognition, Las Vegas, NV, USA, 27–30 June 2015; pp. 770–778. [CrossRef]
34. Howard, A.G.; Zhu, M.; Chen, B.; Kalenichenko, D.; Wang, W.; Weyand, T.; Andreetto, M.; Adam, H. MobileNets: Efficient convolutional neural networks for mobile vision applications. *arXiv* **2017**. [CrossRef]
35. *KS B 0801: 2022*; Test Pieces for Tensile Test for Metallic Materials. Korean Agency for Technology and Standards: Seoul, Republic of Korea, 2022.